JTTEE5 16:886–892
DOI: 10.1007/s11666-007-9076-x
1059-9630/$19.00 © ASM International

Peer Reviewed

Rapid and Continuous Deposition of Porous Nanocrystalline SnO_2 Coating with Interpenetrating Pores for Gas Sensor Applications

K. Chien and T.W. Coyle

(Submitted March 13, 2007; in revised form June 29, 2007)

In this article, we proposed a rapid and continuous process for the production of nanoporous coatings for functional applications. Experiments following two statistical designs were implemented to screen and investigate the spraying parameters' effects on coating crystallinity and porosity in order to gain a better understanding. The spraying standoff distance, solution flow rate and power were identified as having significant effects on coating porosity and crystallinity. The result yielded a peculiar microstructure comprised of interpenetrating pores and layered structures with embedded pores. A deposition mechanism was postulated to explain this microstructure. Ethanol gas sensors that are constructed from the coatings had comparable sensitivities to those reported in the literature for thick-film coatings and had a maximum sensitivity near 200 °C.

Keywords gas sensors, nanocrystalline, plasma spray, solution precursor

1. Introduction

Nanoporous thick film coatings offer high specific surface-area structures, which often improve the sensitivity of resistive-type gas sensors. The production of these coatings typically involves several processes and usually starts with spray prolysis for controlled nanoparticle fabrication with low levels of impurities (Ref 1). Subsequently, the nanoparticles are collected, dispersed in a solvent, screen-printed onto a substrate, heated to dry off volatile species, and sintered to acquire adequate mechanical strength. It is a batch-based production. Therefore, a new technique for rapid and continuous production of nanoporous coatings would be highly desirable. Previous research has rarely examined ways to eliminate steps and reduce porous coating production cycles (Ref 2-4). This article proposes a process that integrates spray pyrolysis, screen-printing, and sintering steps into a single continuous process—solution precursor plasma spray.

1.1 Solution Precursor Plasma Spray (SPPS)

Solution precursor plasma spray is a thermal spraying process that uses thermal plasma as the heat source and aqueous chemical solutions as feedstock instead of powders. The SPPS has many of the advantages in producing narrow particle-size range powder with controlled particle morphologies as combustion flame spray pyrolysis. Furthermore, SPPS is a more flexible process than combustion flame pyrolysis, for example, production and/or deposition of Si-C-N materials is possible, since no oxygen species are involved in the deposition (Ref 5). Also, the melting temperatures of most oxides and ceramic powders are beyond the heating capacity of most combustion flame pyrolysis conditions. The high enthalpy in SPPS is capable of fully melting and even vaporizing high melting temperature materials, allowing for deposition from vapor phase.

1.2 SnO_2-based Gas Sensors

The SnO_2 is one of the most important sensor materials, due to its high sensitivity to toxic and combustible gases. Commercial ethanol and combustible gas sensors are usually SnO_2-base devices (Ref 6, 7). The SnO_2 layer reacts with ambient gas molecules catalytically and/or electrochemically. The SnO_2 surface conductivity increases when reducing molecules are physisorbed and/or chemisorbed on the surface, for example ethanol molecules. Higher concentration of reducing molecules in the atmosphere induces higher SnO_2 surface conductivities (Ref 8, 9). Thus, the sensitivity of this type of gas sensor is defined as R_a/R_g, where R_a is the resistance in air and R_g is

This article is an invited paper selected from presentations at the 2007 International Thermal Spray Conference and has been expanded from the original presentation. It is simultaneously published in *Global Coating Solutions, Proceedings of the 2007 International Thermal Spray Conference*, Beijing, China, May 14-16, 2007, Basil R. Marple, Margaret M. Hyland, Yuk-Chiu Lau, Chang-Jiu Li, Rogerio S. Lima, and Ghislain Montavon, Ed., ASM International, Materials Park, OH, 2007.

K. Chien and **T.W. Coyle,** Centre for Advanced Coatings and Technologies, University of Toronto, Toronto, ON, Canada. Contact e-mail: ksquare.chien@utoronto.ca.

the resistance in the controlled testing atmosphere. This definition implies that larger specific-surface-area materials contain more gas/solid interaction sites. Therefore, the sensitivity of the sensors is directly related to the specific surface area.

Moreover, nanocrystalline coatings improve sensitivity (Ref 10). The improvement is related to particle size, since the change in conductivity only happens within a thin depletion layer, a region depleted of major charge carriers. The depletion layer depth (D_d) is only a few nanometers from the surface and is independent of particle size. If the particle is large, only the skin of the particle is affected. If the particle size is reduced to twice of D_d, the entire particle's conductivity is altered, which leads to an additional contribution to the sensitivity. Thus, the sensitivity increases dramatically when the particle size is smaller than 10 nm (Ref 11).

The operating temperatures for the sensors are ranging from 200 to 400 °C. The sensitivity has a peak around 300 °C. The low sensitivity at low temperature is due to slow kinetic reaction. At high temperatures the base conductivity is saturated, therefore, the change in conductivity becomes insignificant (Ref 12).

2. Experimental Procedure

2.1 Preparation of Solution and Spray Set-up

A solution injector consisting of a Swagelok (Swagelok, OH, USA) union tee connector, an inner needle with 0.5 mm inner diameter and an outer needle with 1.2 mm inner diameter as a coaxial air-blast atomizer were constructed. The solution precursor was prepared by mixing $SnCl_4 \cdot 5H_2O$ with distilled water to desired concentrations. Compressed air generated atomized solution droplets, and the momentum of the air carried and injected the droplets into a DC plasma jet as shown in Fig. 1. The exit of the injector was positioned 10 mm downstream of the plasma gun and 10 mm above the plasma centerline. The deposition time was 5 min for all spraying conditions.

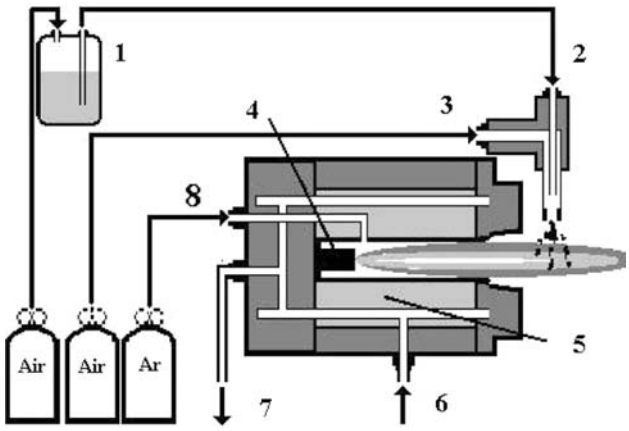

Fig. 1 Experimental set up. (1) Pressurized solution vessel, (2) solution inlet, (3) compressed air inlet, (4) cathode, (5) anode, (6) cooling water inlet, (7) cooling water outlet, and (8) Ar gas inlet

A Taguchi Design of Experiments (DOE) approach was used to identify the parameters having significant influence on the coating porosity and crystallinity. The investigated parameters were solution flow rates, solution concentrations, operating currents, standoff distances, atomizing pressures, and Argon flow rates. Table 1 provides high and low conditions for the screening. A Uniform DOE was then used to optimize the effects of the significant parameters in greater detail.

The coating morphologies, microstructures, and porosities were examined and measured using a scanning electron microscope, scanning transmission electron microscope, energy dispersive x-ray analysis, and mercury-intrusion techniques.

2.2 Sensitivity Measurement

The coated disks were cut into 2 cm by 1 cm rectangles, electrical contacts were made across the length of the specimen at both ends with silver paste, and the specimen was then placed in a cylindrical quartz tube inside a tube furnace. Figure 2 illustrates that the resistance along the

Table 1 Screening parameter conditions

	High	Low
Solution flow rate (mL/min)	35	25
Solution concentration (M)	0.25	0.15
Operating current (A)	600	500
Stand-off distance (cm)	10	6
Atomizing pressure (psi)	25	15
Argon gas flow rate (L/min)	60	50

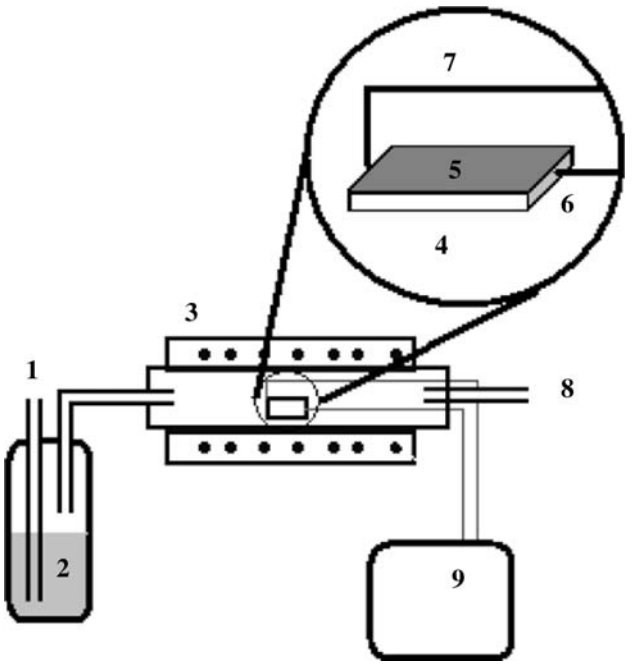

Fig. 2 Sensitivity measurement. (1) Dry air in, (2) ethanol solution, (3) tube furnace, (4) substrate, (5) SnO_2 coating, (6) silver past, (7) electrodes, (8) exhaust gas, and (9) data acquisition system

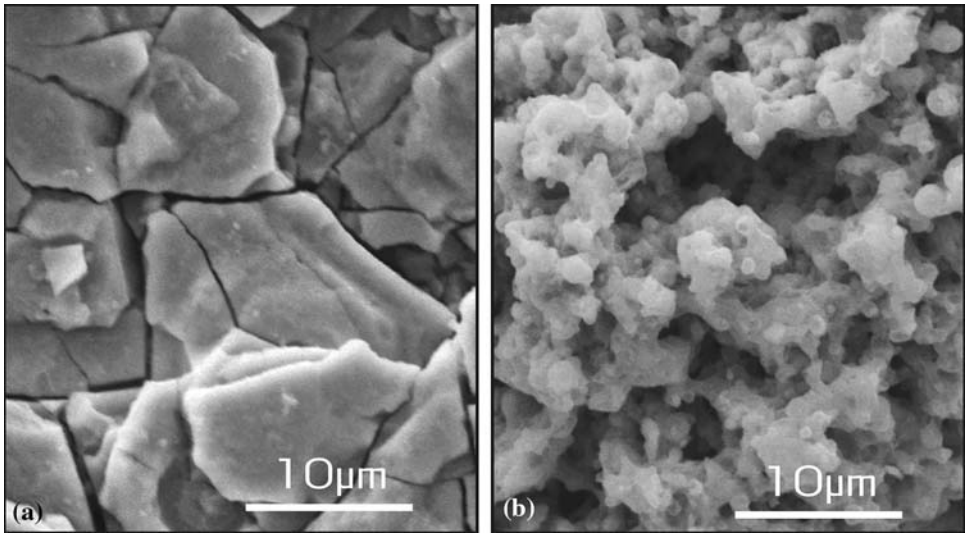

Fig. 3 Surface morphologies of as-sprayed coatings. (a) Dense and (b) powdery

length of the SnO_2 coating was measured through two electrodes using a data acquisition device. The sensitivity was calculated using the R_a/R_g ratio.

The measurement went through three steps, dry air → air + ethanol gas → air as one cycle. Each step was held for 30 min at 100 cc/min flow rate. Several measurements were done between 150 and 300 °C.

3. Results

Analysis of variance for Taguchi DOE identified solution flow rates, power settings and standoff distance, as the most influential parameters on porosity, crystallinity, and deposition efficiency.

3.1 Taguchi DOE

Figure 3(a) and (b) exemplifies two different coating morphologies by varying the influential parameters identified by Taguchi. The coating deposited with all high level settings of the three parameters is dense and shown in Fig. 3(a). This coating has the lowest substrate temperature, almost amorphous crystal structure and both the highest deposition efficiency, and residual Cl contents. The porous coating, deposited under all low level settings, is shown in Fig. 3(b). The coating has little coherence between particles and difficulty in handling and depositing silver electrodes on it. Figure 4 provides the substrate temperatures information for different types of coating morphologies.

3.2 Uniform DOE

Table 2 lists the details of the condition which resulted in the highest ethanol sensitivity based on the Uniform design optimization runs. Figure 5 shows the optimal coating is nanocrystalline. The crystallite size is calculated using the Scherrer equation with Al_2O_3, as a reference peak to eliminate the effect of instrumental broadening (Ref 13). The calculated grain size is less than 10 nm.

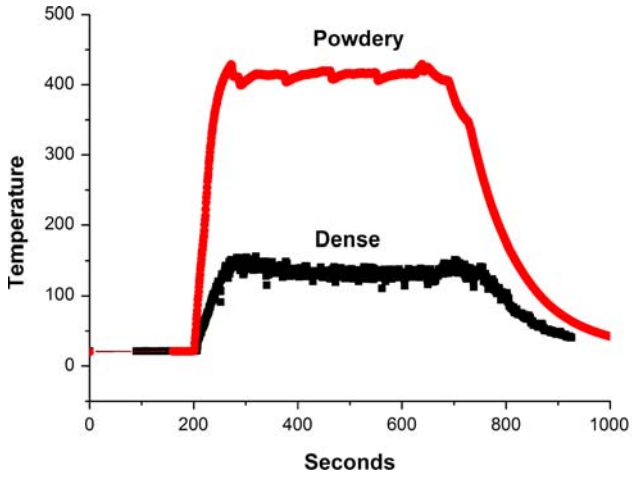

Fig. 4 Typical substrate temperature profiles during spraying

Table 2 Optimal deposition conditions

	Conditions
Solution flow rate (mL/min)	25
Gun current (A)	520
Stand off distance (cm)	9
Solution concentration (M)	0.25
Plasma flow rate (L/min)	50
Atomizing pressure (Psi)	15

The microstructure of the coating consists of apparent agglomerated particles and pore channels in between them, as can be seen from Fig. 6. The size of the agglomerated particles is around 30 μm. Figure 7 displays a fracture surface that runs through the agglomerates, the pores are shown with white dashed lines. As can be seen from this fractograph, the apparent agglomerates consist

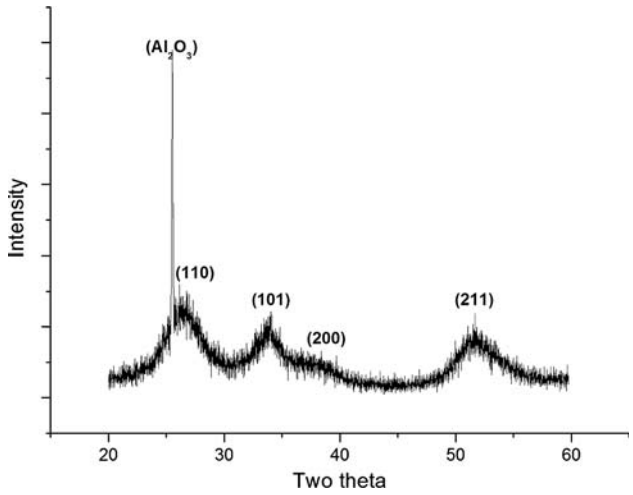

Fig. 5 An XRD pattern of the SnO_2 coating

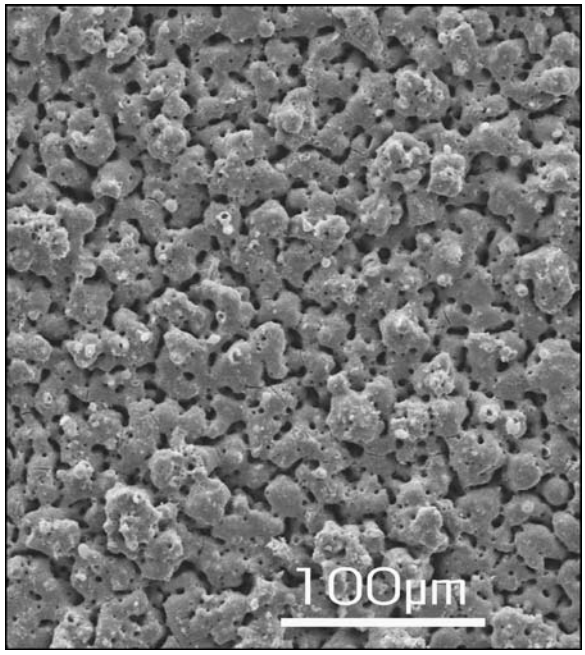

Fig. 6 Morphology of the SnO_2 coatings

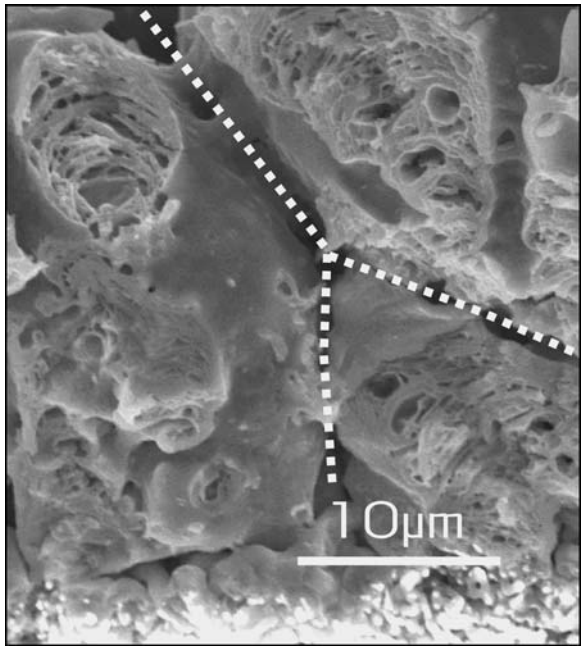

Fig. 7 A SEM image of a fractured coating

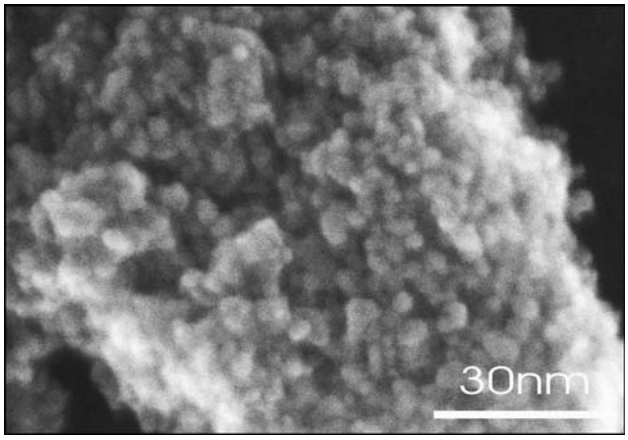

Fig. 8 STEM image of SnO_2 coatings

of a layered structure with pores embedded between layers. The thickness of these layers is less than 1 μm.

Figure 8 reveals the layers to be comprised of nanoparticles. The calculated average particle size from STEM images is 6.9 nm, which is in close agreement with the XRD estimation. The porosity and surface area of the coating are 42% and 154 m^2/g, respectively. Figure 9 shows two sensor responses with optimized and conventional conditions. All the measurements are done above 150 °C to avoid possible interference from condensed water on the SnO_2 surface. It can be seen that the optimized coating has a peak sensitivity around 200 °C and higher sensitivity peak. The other has a maximum temperature around 300 °C and much lower sensitivity—which is close to pure SnO_2 sensors fabricated by precipitation and then sintering (Ref 14).

4. Discussion

All the coatings are deposited under relatively lower power settings, 15-20 kW, and longer stand-off distances compared to dense thermal barrier coatings produced by solution precursor and suspension plasma spraying

(Ref 15). Thus, there might be very little molten particles and splats, and most of them are gel-like viscous precursor arriving on substrates. The precursor is then pyrolyzed from the heat flux of plasma jet while on substrates, resulting in high Cl content, numerous surface cracks and almost amorphous coatings as can be seen in Fig. 3(a). The microstructure and crystallinity is very close to spray pyrolysis SnO_2 coatings with a 150 °C substrate temperature. Figure 3(b) suggests most of the precursor is pyrolyzed and partially molten with little coherence. The coating is powdery and found in the cold periphery region of the plasma jet in solution precursor sprayings. The optimal deposition condition is between spray pyrolysis and solution plasma spraying due to high solution flow rate and low power settings. Some unique microstructures could be found under this intermediate condition.

The coating which has the highest sensitivity consists of interpenetrating pores separating agglomerated particles which themselves have thin layers enclosing micropores.

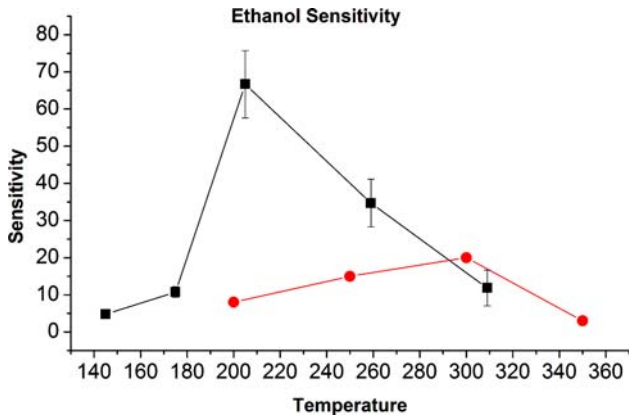

Fig. 9 Ethanol sensitivity

Each layer is composed of SnO_2 nanoparticles. There are some observable microcracks between two adjacent agglomerates on the coating surface. The microcracks are formed due to the tensile stress derived from the pyrolysis of residual precursor (Ref 16). The pores channels and microcracks are advantageous for a gas sensor. The whole coating becomes accessible to ambient gases and enhances the sensitivity of the coating. Thus the coating has good ethanol sensitivities at a lower maximum sensitivity temperature (Ref 17-19).

Figure 10(a) shows a hollow sphere positioned on top of many layers enclosing a micropore. Figure 10(b) illustrates that most of the layers are highly distorted and wrapping around a large pore or hollow sphere. The highly contorted layers enclosing distorted pores are not typically seen in solution precursor plasma sprayed coatings. In order to investigate the formation of the coating, deposits were collected on glass slides by quickly passing them through the plasma jet. It can be seen in Fig. 11(a), that some deposits collected at 8 cm from the plasma gun were ruptured hollow particles 2-3 μm in diameter-no evidence of molten particles or splats was observed. Figure 11(b) shows most of the collected particles are around 2-3 μm, some particles could be 6-10 μm. Figure 11(c) displays all the apparent solid particles are melted after annealing at 350 °C, except some ruptured hollow particles. Most of the particles are melted at relatively low temperature suggesting that particles arriving on substrates are either $SnCl_2$ or $SnCl_4 \cdot 5H_2O$.

The distortion of pores, nano-particle layers and melting of collected particle at low temperature lead to the suggestion of a new possible deposition mechanism. It is postulated that the majority of the particles impacting the substrate are still un-pyrolyzed or partially pyrolyzed tin salt particles. Only the ruptured particles and a few solid particles are completely pyrolyzed into SnO_2, which has much higher melting point. The solution droplets traveling

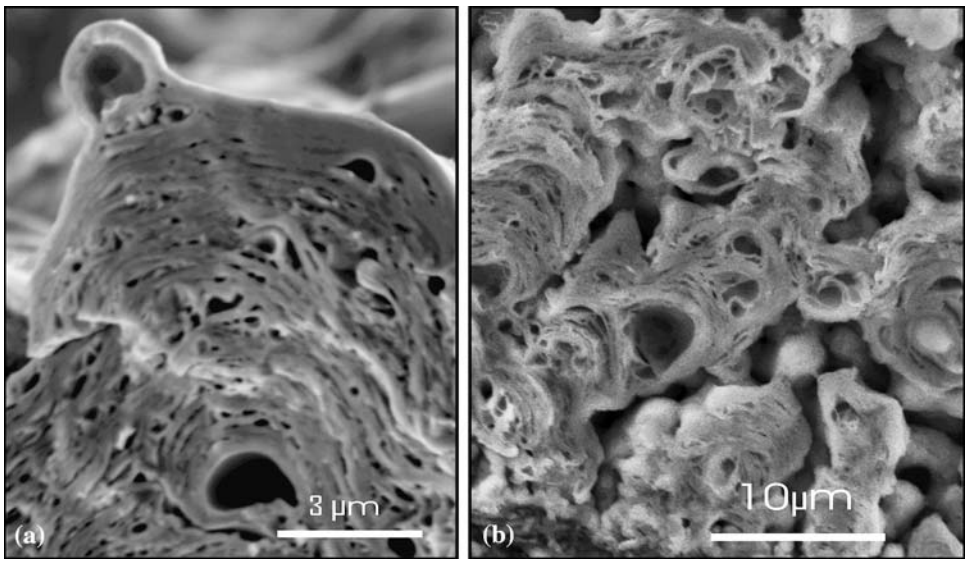

Fig. 10 Distorted thin layer. (a) Layered particles and (b) distorted layers

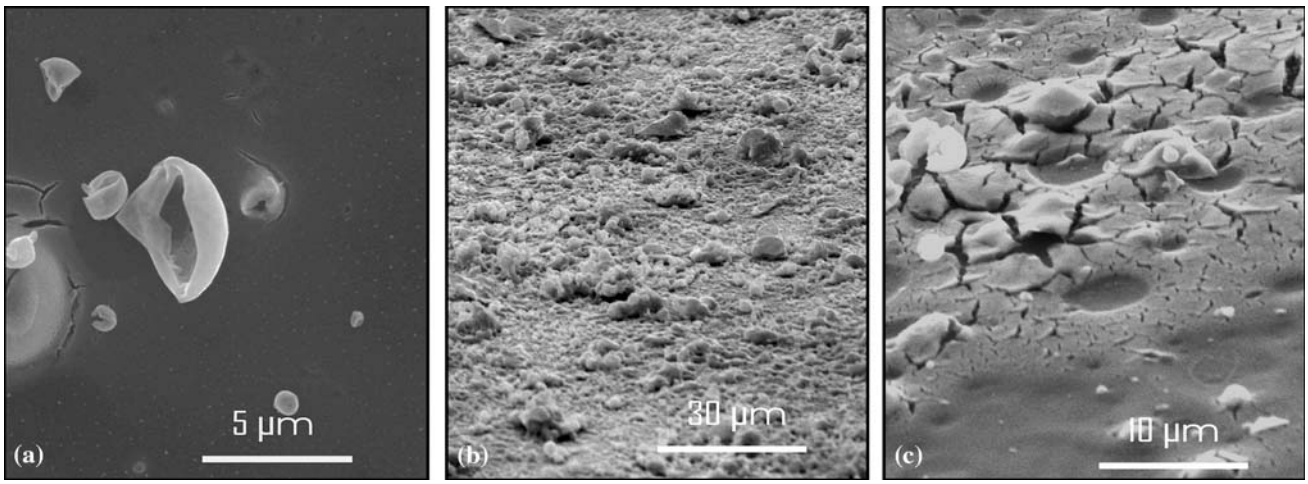

Fig. 11 Un-pyrolyzed particles. (a) Ruptured hollow spheres, (b) 2-3 μm particle size, and (c) annealed

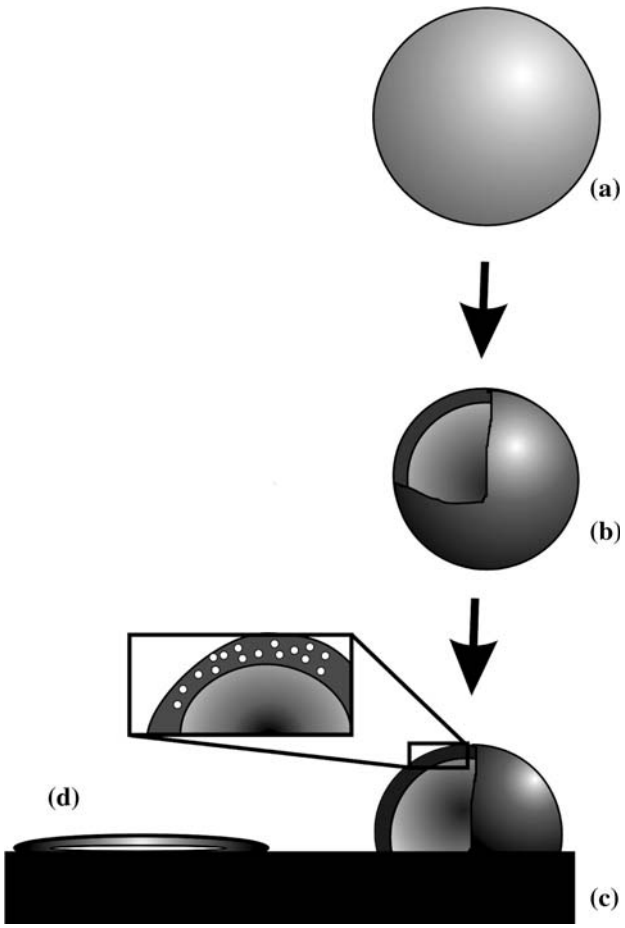

Fig. 12 Schematic representation of a single droplet depositing on a substrate

from the exit of the solution injector toward the substrates undergo rapid evaporation. The relatively low concentration of the solution and continuous removal of water from the droplet may result in increase of the viscosity of the droplet. Rapid evaporation of the surface solvent results in surface precipitation of the metal salts, as shown in Fig. 12(a) and (b). These viscous spheres deform upon impact on the substrate, pyrolyze and then crystallize into nanocrystalline rutile SnO_2 in situ under the plasma heat flux, as shown in Fig. 12(c). The viscous droplets may deform into flat discs or wrap around rigid hollow SnO_2 particles by their own momentum and/or by subsequent impact of particles before they pyrolyze, as shown in Fig. 12(d). Thus, the embedded micro-pores are ruptured hollow SnO_2 particles or hollow SnO_2 spheres. The pyrolysis of the residual precursor results in microcrack formation in the coatings.

5. Conclusion

An aqueous $SnCl_4$ solution feedstock was used to integrate the spray pyrolysis and sintering of nano SnO_2 particles in nanoporous coating production. The coating consists of interpenetrating pores separating agglomerated particles which themselves consist of a layered structure with micropores between the layers. Each layer is comprised SnO_2 nanoparticles. The structure was apparently formed from overlapping viscous hollow spheres of Sn solution which were pyrolyzed and annealed in situ. The coatings show high porosity and specific surface areas. Sensors constructed directly from the porous coatings have good ethanol gas sensitivity at 200 °C.

References

1. J.H. Kim, V.I. Babushok, T.A. Germer, G.W. Mulholland, and S.H. Ehrman, Co-solvent Assisted Spray Pyrolysis for the Generation of Metal Particles, *J. Mater. Res.*, 2003, **18**, p 1614-1622
2. H. Zahir, K. Sato, and Y. Iwamoto, Development of Hydrothermally Stable Sol-gel Derived La_2O_3-doped Ga_2O_3-Al_2O_3 Composite Mesoporous Membrane, *J. Membr. Sci.*, 2005, **247**, p 95-101

3. C.M. Li, H. Lei, Y.J. Tang, J.S. Luo, and Z.M. Chen, Production of Copper Nanoparticles by the Flow-levitation Method, *Nanotechnology*, 2004, **15**, p 1866-1869
4. S. Maenosono, T. Okubo, and Y. Yamaguchi, Overview of Nanoparticle Array Formation by Wet Coating, *J. Nanopart. Res.*, 2003, **5**, p 5-15
5. J. Wilden, A. Wank, and M. Asmann, Synthesis of Si-C-N by Thermal Plasma Jet Chemical Vapor Deposition Applying Liquid Precursors, *Appl. Organomet. Chem.*, 2001, **15**, p 841-857
6. G. Sberveglieri, Recent Development in Semiconducting Thin-film Gas Sensors, *Sens. Actuators B*, 1995, **23**, p 103-109
7. J. Ge, J. Wang, H. Zhang, X. Wang, Q. Peng, and Y. Li, High Sensitive SnO_2 Microspheres, *Sens. Actuators B*, 2006, **113**, p 937-943
8. N. Barsan, R. Grigorovici, R. Ionescu, M. Motronea, and A. Vancu, Mechanism of Gas Detection in Polycrystalline Thick Film SnO_2 Sensors, *Thin Solid Film*, 1989, **71**, p 53-63
9. D.F. Cox, T.B. Fryberger, and S. Semancik, Oxygen Vacancies and Defects Electronics States on the SnO_2 (110)-1X1Surface, *Phys. Rev. B*, 1998, **38**, p 2072-2083
10. G. Zhang and M. Liu, Effect of Particle Size and Dopant on Properties of SnO-based Gas Sensors, *Sens. Actuators B*, 2000, **69**, p 144-152
11. C. Xu, J. Tamaki, N. Miua, and N. Yamazoe, Grain Size Effects on Gas Sensitivity of Porous SnO_2-bases Elements, *Sens. Actuators B*, 1991, **3**, p 147-155
12. D. Cox, T. Fryberger, and S. Memancik, Oxygen Vacancies and Defect Electronics States on the SnO_2 (110)-1X1 surface, *Phys Rev. B*, 1998, **38**, p 2196
13. D.J. Dyson, X-ray and Electron Studies in Materials Science. Maney, London, 2004
14. T. Jinkawa, G. Sakai, J. Tamaki, N. Miura, and N. Yamazoe, Relationship between Ethanol Gas Sensitivity and Surface Catalytic Property of Tin Oxide Sensors Modified with Acid or Basic Oxides, *J. Mol. Catal. A*, 2000, **155**, p 193-200
15. P. Fauchais, V. Rat, C. Delbos, J.F. Coudert, T. Chartier, and L. Bianchi, Understanding of Suspension DC Plasma Spraying of Finely Structured Coatings for SOFC, *IEEE T. Plasma Sci.*, 2005, **33**, p 920-930
16. L. Xie, D. Chen, E. Jordan, A. Ozturk, F. Wu, X. Ma, B. Cetegen, and M. Gell, Formation of Vertical Cracks in Solution Precursor Plasma Sprayed Thermal Barrier Coatings, *Surf. Coat. Technol.*, 2006, **201**, p 1058-1064
17. O.K. Tan, W. Cao, Y. Hu, and W. Zhu, Nanostructured Oxides by High Energy Ball Milling Technique: Application as Gas Sensing Materials, *Solid State Ionic*, 2004, **172**, p 309-316
18. D. Kotsikau, M. Ivanovskaya, D. Orlik, and M. Falasconi, Gas-sensitive of Thin and Thick Film Sensors Based on Fe_2O_3-SnO_2 Nanocomposite, *Sens. Actuators B*, 2004, **101**, p 199-206
19. F. Hellegouarc'h, F. Arefi-Khonsari, R. Planade, and J. Amouroux, PECVD Prepared SnO_2 Thin Films for Ethanol Sensors, *Sens. Actuators B*, 2001, **73**, p 27-34